GHGT-12

CO₂ -Plume Geothermal (CPG) Heat Extraction in Multi-layered Geologic Reservoirs

Nagasree Garapati[a], Jimmy B. Randolph[a,b], José L. Valencia Jr.[a], and Martin O. Saar[a,b]*

[a]Department of Earth Sciences, University of Minnesota – Twin Cities, Minneapolis, MN 55455, USA
[b] TerraCOH Inc, 1409 Washington Ave N, Minneapolis, MN 55411, USA

Abstract

CO₂-Plume Geothermal (CPG) technology involves injecting CO_2 into natural, highly permeable geologic units to extract energy. The subsurface CO_2 absorbs heat from the reservoir, buoyantly rises to the surface, and drives a power generation system. The CO_2 is then cooled and reinjected underground. Here, we analyze the effects of multi-layered geologic reservoirs on CPG system performance by examining the CO_2 mass fraction in the produced fluid, pore-fluid pressure buildup during operation, and heat energy extraction rates. The produced CO_2 mass fraction depends on the stratigraphic positions of highly permeable layers which also affect the pore-fluid pressure drop across the reservoir.

Keywords: carbon dioxide; geothermal system; reservoir simulations; heterogeneity; brine displacement; carbon capture and sequestration (CCS); carbon capture utilization and sequestration (CCUS).

1. Introduction

The CO₂ Plume Geothermal (CPG) [1-5] energy capture and conversion cycle begins with the collection of CO_2 gas from an emitter such as a fossil-fuel power plant, chemical factory, ethanol plant, cement manufacturer, or other sources. The captured CO_2 is then injected into high-permeability sedimentary and stratigraphic basins to extract heat from the subsurface. These basins are bound by base and caprock formations of low permeability, as seen in Fig. 1. The injected CO_2 forms a large subsurface plume that absorbs heat from the geothermal reservoir, is pumped to the surface for thermal and/or electric power production [2-4, 6, 7], and is then cooled and re-injected into the subsurface.

---

* Corresponding author. Tel.: +1-612-625-7332; fax: +1-612-625-3819.
  E-mail address: saar@umn.edu

The heat density of sedimentary basins is relatively low when compared to artificially hydro fractured, smaller-scale reservoirs [8]. This detriment, however, is likely overcome by the large accessible volume of natural reservoirs, allowing the total heat energy output of natural reservoirs to potentially surpass that of artificial basins. Furthermore, supercritical CO_2 has a high mobility (i.e., low kinematic viscosity) and high thermal expansibility compared to water, resulting in the formation of a strong thermosiphon [6, 9, 10] that typically eliminates parasitic pumping requirements. Both effects tend to significantly increase electricity production efficiency. Another benefit of the CPG system is that it is a closed-loop cycle, inhibiting the release of CO_2 into the atmosphere. The CPG cycle involves combining the produced CO_2 with the CO_2 sequestration stream from the emitter, thus creating a negative carbon footprint by operating as a CO_2 sequestering geothermal power plant [1-3]. In addition to a negative carbon footprint, CPG has operational flexibility as it can be operated with a finite amount of underground-stored CO_2, removing the need for additional, continuous CO_2 injection and geologic CO_2 storage if it is impractical or uneconomic under some conditions [11]. Such scenarios are investigated here, where initially the CO_2 plume is developed by injecting CO_2 into the reservoir. Thereafter, CO_2 is produced and circulated in a closed loop without further addition of CO_2. An additional benefit is the system's ability to handle the ramping up or down of the produced CO_2 stream. Controlling the thermosiphon can increase system longevity by slowing the rate of heat depletion within the reservoir. This rate is not only contingent upon the movement of both the free-phase CO_2 and the dissolved CO_2, but its sensitivity to variations in permeability. Once optimized for a specific region or geologic reservoir, a CPG system can provide important economic and environmental gains.

Fig. 1. Simplified schematic of one possible implementation of a CO_2-Plume Geothermal (CPG) system (modified from Randolph and Saar [3]; Saar et al. [4]), established in a deep saline aquifer.

Here, we analyze the effects of multi-layered, i.e., vertically heterogeneous, geothermal reservoirs on CPG system performance by examining 1) the CO_2 mass fraction in the produced fluid (target of at least 94%, Welch and Boyle [12]), 2) the reservoir pore-fluid pressure build-up during operation, and 3) heat energy extraction rates. The reservoir is divided into two, three, or four horizontal geologic layers each layer with a different horizontal permeability, k_x.

The vertical permeability, k_z, is adjusted to maintain the same anisotropy ratio of $k_x/k_z = 2$ in all scenarios. More details are provided in Section 2.

2. Numerical Model:

In keeping with the objective of formulating a simple model to gain first-order insights, we assume a layered reservoir with symmetrical CO_2 plume formation around the injection well. The current model is radially axisymmetric and employs a cylindrical coordinate system (Fig. 2), which reduces the computational efforts when compared to some previous simulations [1-3]. This axisymmetric model is modified from Garapati et al. [11] to include layers. We employ the numerical simulator TOUGH2 [13, 14] with the equation of state (EOS) module ECO2N [15].
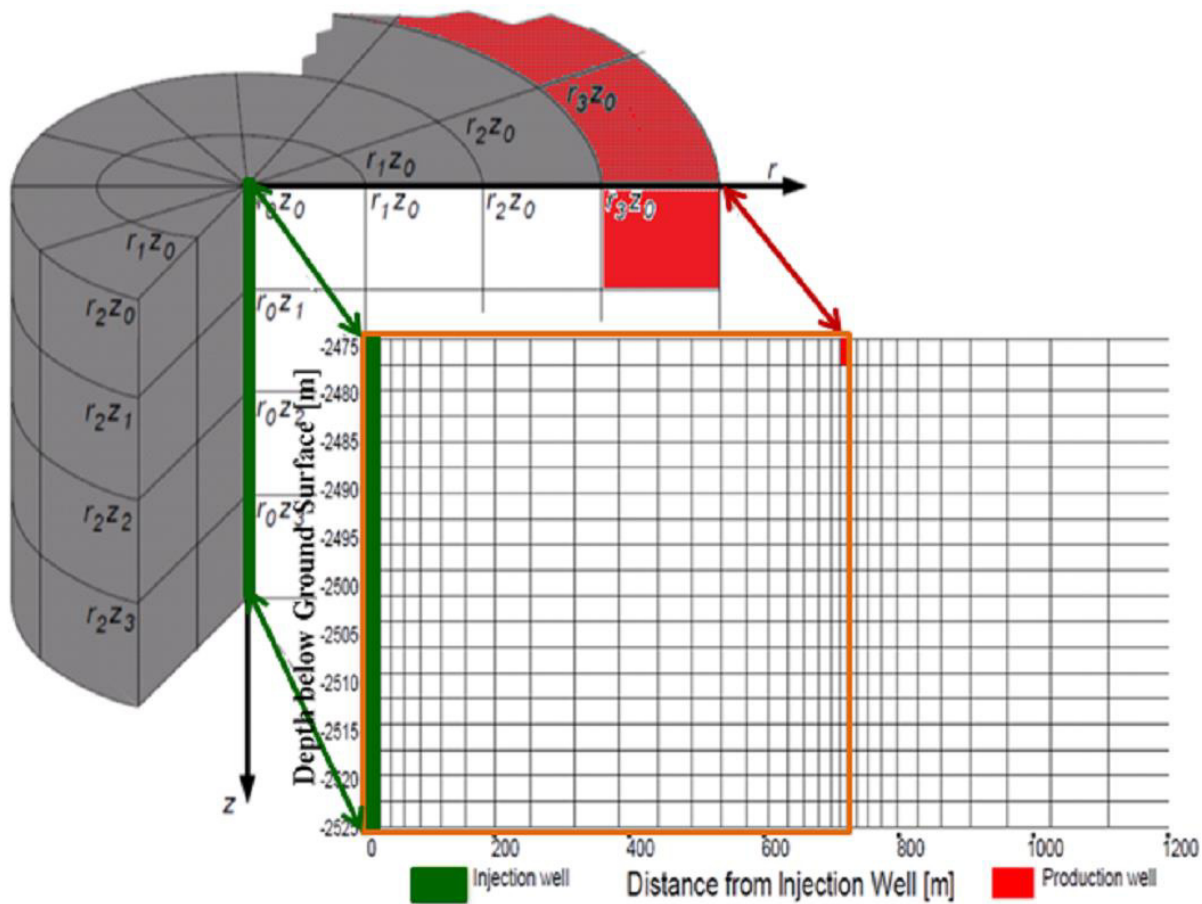
Fig. 2. Three-dimensional (3D), axisymmetric model with a cross section of the geothermal reservoir showing grid discretization and well placement. The caprock bottom is located at a depth of 2475 m. The injection well is vertical and fully penetrating within the reservoir and constitutes the axis of symmetry. The production well is horizontal, circular and located just below the caprock at a distance from the injection well (here shown are 707 m). The model extends horizontally to 100 km to minimize boundary effects, with logarithmically increasing horizontal grid spacing away from the injection well but horizontal refinement of grid spacing near the production well. Modified from Garapati et al. [11] through inclusion of geologic layers (see Fig. 3).

The reservoir model is considered to be 100 km in radius, 50 m thick and located at an average depth of 2.5 km with a uniform porosity of 0.10. The radius is chosen to permit no-flow lateral boundary conditions. The upper and lower

reservoir boundaries are also assumed to permit no-fluid flow, although semi-analytic heat transfer [13] is permitted to represent the cap rock and bed rock surrounding the reservoir. The CO_2 enters the reservoir from a linear vertical injection well, which constitutes the axis of symmetry. After moving through the geothermal reservoir, the heated CO_2 is produced from a horizontal well located at the top of the reservoir at 707 m from the injection well. This allows the CO_2 extraction operations to take advantage of CO_2 buoyant flow and maximize CO_2 recovery while minimizing unwanted brine extraction (Fig. 2). Although it constitutes a simplified geometry, the radial configuration accurately captures physical CO_2/brine multi-fluid behavior, including modern fluid production from a horizontal production well, while permitting efficient numerical modelling [11]. The reservoir is divided into two, three, or four horizontal geologic layers, each layer with a different horizontal permeability, k_x, as shown in Fig. 3. The vertical permeability, k_z, is adjusted to maintain the same anisotropy ratio, k_x/k_z, in all scenarios. In a two-layered system, a total of four cases are considered. The first two cases have a low-permeability layer at the top with a different horizontal permeability ratio, $k_x(1)/k_x(2)$. The top and bottom layers are inverted for the last two cases. In three- and four-layered systems, different cases of a) increasing permeability of layers with depth, b) decreasing permeability with depth, and c) alternate layers of high and low permeability layers are considered. Table 1 lists additional details about the model setup, including the use of a standard semi-analytic conductive heat exchange boundary condition to over- and underlying layers [13] along with numerical model parameters.
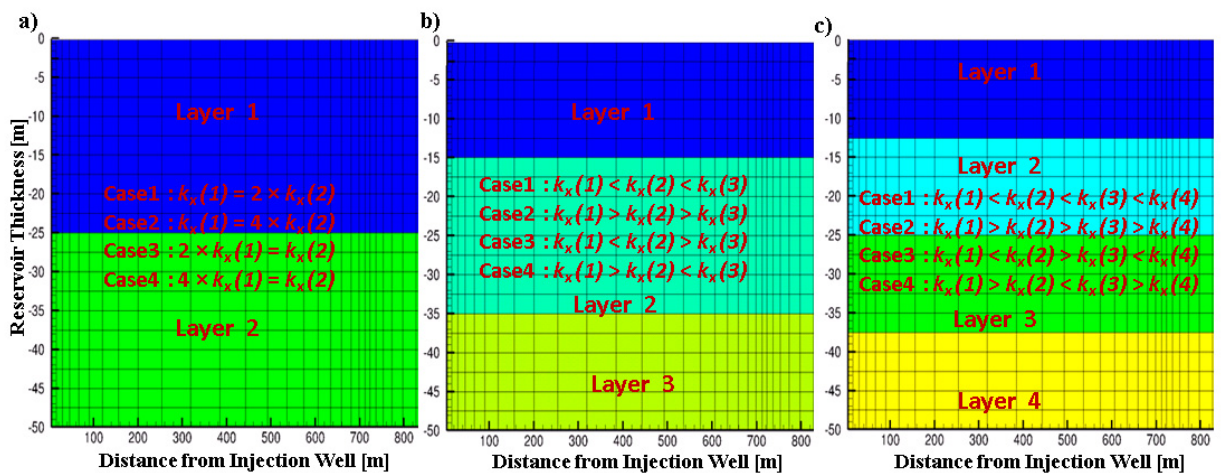
Fig. 3. Multi-Layer reservoir model with a) two layers, b) three layers, and c) four layers.

Table 1. Numerical model parameters for the base case.

Model Parameter/Condition	Value
Number of grid cells, vertical	20
Numerical grid configuration	Radially symmetric about the injection well
Well spacing	707 m
Well orientation	Vertical (injection), horizontal circular (production)
Boundary conditions (top/bottom)	No fluid flow, semi-analytic heat exchange
Boundary conditions (lateral)	No fluid or heat flow (with model extending 100 km)
Initial conditions	Hydrostatic equilibrium, all pore space occupied by brine

As discussed in Garapati et al. [11], initially, the reservoir is assumed to be filled with native brine with an NaCl saturation of 20% mass fraction. During the simulation, the CO_2 plume is developed over 2.5 years by injecting 2 Mtons of CO_2 at a rate increasing linearly from 0 to 1 Mton/year over the first year and then at a constant rate of 1

Mton/yr for an additional 1.5 yrs. As mentioned in the introduction, once the plume is fully formed, injection of CO_2, initially collected from emitters is stopped and fluid (mostly CO_2) production and circulation is initiated. The circulation rate is increased linearly over 2 years and then maintained at a constant rate for an additional 98 years. Tables 2 and 3 list the geologic conditions of the reservoir and reservoir-fluid parameters, respectively. Randolph and Saar [2, 3] provide further explanations for the choice of specific base case reservoir parameters.

Table 2. Reservoir physical parameters for the base case.

Reservoir Parameter/Condition	Value
Average depth, D [m]	2500
Anisotropy ratio, k_x/k_z	2
Thermal conductivity [W/m/^{0}C]	2.10
Thickness [m]	50
Temperature, T [^{0}C]	100
Porosity	0.10
Rock specific heat [J/kg/^{0}C]	1000
Rock grain density [kg/m^3]	2650
Radius [m]	100,000
Background geothermal gradient [^{0}C/km]	34

Table 3. Reservoir fluid parameters.

Fluid Property	**Value**
Residual brine saturation fraction	0.30
van Genuchten parameter for two-phase flow, m	0.457
Native brine NaCl saturation [ppm]	200,000
Residual CO_2 saturation	0.05
van Genuchten parameter for two-phase flow, a [1/Pa]	5.1×10^{-5}

3. Results

In the following, we present results for two-, three-, and four-layered reservoir systems (Fig. 3) with respect to CO_2 mass fraction in the produced fluid, which is ideally maximized, pore-fluid pressure build-up during operation, which is ideally minimized, and heat energy extraction rates. While the main discussion of each system is provided along with each respective result, Section 4 provides a summary discussion of the effects of layers on produced CO_2 mass fraction, pore-fluid pressure evolution, and heat extraction rates.

3.1. Two- Layered System

In the two-layered system simulated, four cases are considered (Fig. 3). The first two cases exhibit a bottom layer permeability of 4×10^{-14} m^2 and 8×10^{-14} m^2, respectively, and include the same top layer permeability of 2×10^{-14} m^2. The top and bottom layers are then inverted for the last two cases, as shown in Figs. 3 and 4. The effects that layer thickness and permeability have on the mass fraction of CO_2 in the produced fluid can be seen in Figs. 4 and 5. Additionally, the pore-fluid pressure differences just below the caprock between injection and production wells for different horizontal layer thicknesses are shown in Fig. 6. In all these figures, h_1 is the thickness of the top layer and bottom layer thickness, h_2, is 50m – h_1.

Figs. 4a and 4b, show the effect of horizontal layer thickness on CO_2 mass fraction in the produced fluid for the first two cases with a top low-permeability layer and a permeability heterogeneity ratio of 2 and 4, respectively. As the thickness of the bottom layer increases, the CO_2 concentration in the produced fluid decreases. The effect is more

pronounced for high permeability ratios as the radial flow dominates over buoyancy flow, as seen in Fig. 5 (which represents the CO_2 saturations in the reservoirs after the initial injection period for layers with equal thicknesses). Figs. 4c and 4d show the results for cases with a low-permeability layer at the bottom. Here, the top layer has a more pronounced effect on CO_2 saturation, with some effect resulting from the bottom low-permeability layer. The pore-fluid pressure drop decreases in all cases as the thickness of the high-permeability layer increases. This effect is most pronounced when the high-permeability layer is at the top of the reservoir as seen in Fig. 6.
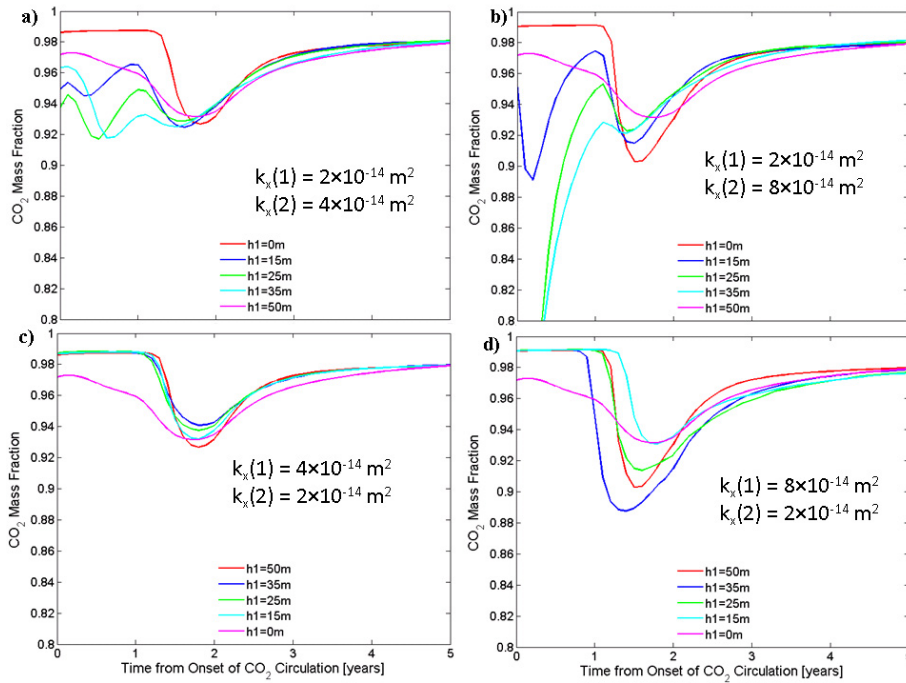
Fig. 4. Produced CO_2 mass fraction over time for different horizontal layer thicknesses, h, and with the low-permeability layer at the top with a) $k_x(2)/k_x(1) = 2$ and b) $k_x(2)/k_x(1) = 4$ and with the low-permeability layer at the bottom with c) $k_x(1)/k_x(2) = 2$ and d) $k_x(1)/k_x(2) = 4$. Layers are shown in Fig. 3.
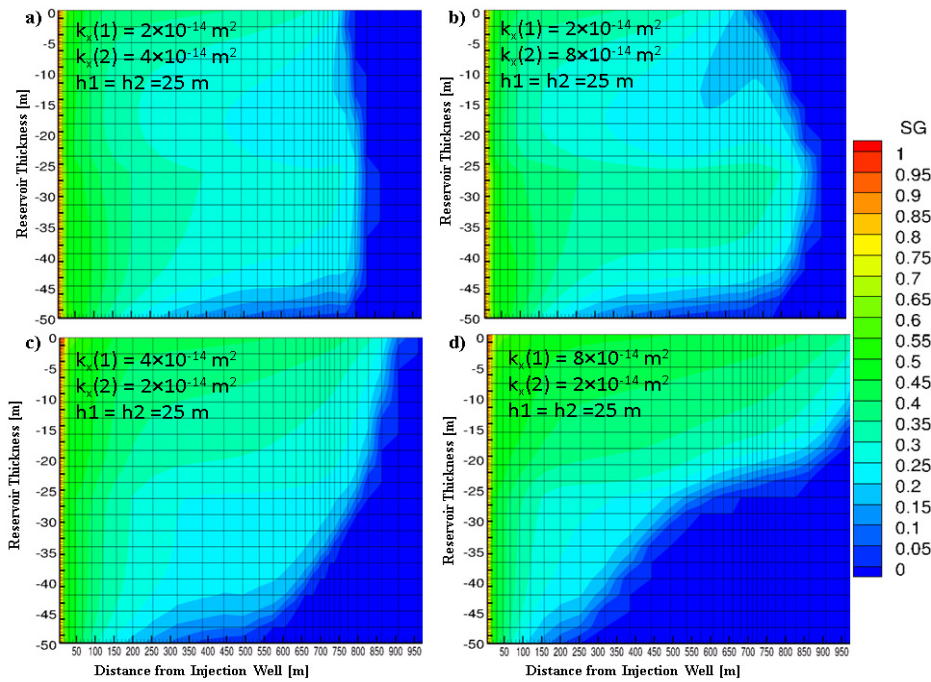
Fig. 5. Radial cross section (as shown in Fig. 2) contour plots of the CO_2 saturation (SG) in the geothermal reservoir pore fluid after initial CO_2 plume formation that results from injection of 2 Mtons of CO_2 over 2.5 years. Shown are cases for layers with equal thicknesses with the low-permeability layer at the top and with a) $k_x(2)/k_x(1) = 2$ and with b) $k_x(2)/k_x(1) = 4$ and with the low-permeability layer at the bottom with c) $k_x(1)/k_x(2) = 2$ and d) $k_x(1)/k_x(2) = 4$.
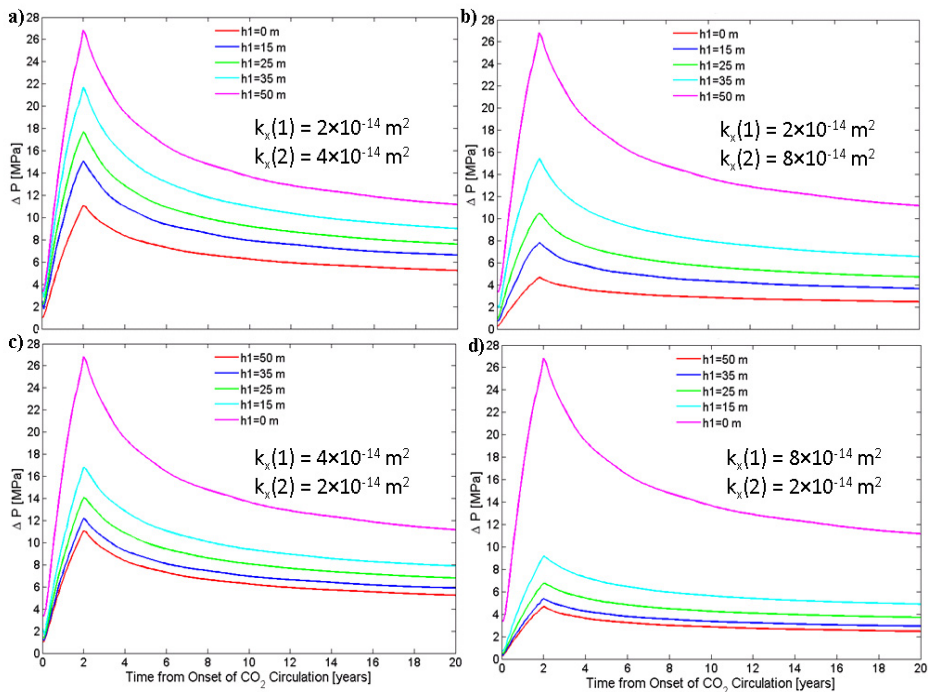
Fig. 6. Pore-fluid pressure drop in the reservoir between the injection and the production wells at the top of the reservoir below the caprock for different horizontal layer thicknesses (Fig. 3) and with the low-permeability layer at the top with a) $k_x(2)/k_x(1) = 2$ and with b) $k_x(2)/k_x(1) = 4$ and

the low-permeability layer at the bottom with c) $k_x(1)/k_x(2) = 2$ and d) $k_x(1)/k_x(2) = 4$.

3.2. Three- Layered System

In the three-layered system simulated, we consider horizontal layers of varying permeability, where each layer has a constant permeability, i.e., the permeability of the layer is not changing across the layer thickness. The layer thickness is fixed at 15 m for the top and bottom layers and set to 20 m for the middle layer. The different cases are: 1) the layer-permeability increases with depth, 2) the layer-permeability decreases with depth, 3) a high-permeability layer is sandwiched between two low-permeability layers, and 4) a low-permeability layer is sandwiched between two high-permeability layers.

The CO_2 mass fraction in the produced fluid and the pore-fluid pressure difference between the injection and production wells for different scenarios are shown in Figs. 7 and 8, respectively. In all scenarios, as the permeability of the highly permeable layer increases, the minimum CO_2 mass fraction in the produced fluid as well as the pressure difference between the well, decreases. When the low-permeability layer is at the top, the CO_2 mass fraction in the produced fluid is affected by the permeability of the bottom layers (Figs. 7a and 7c). In contrast, when the permeability of the top layer is high, the effect of the bottom layer permeability is limited (Figs. 7b and 7d). The pore-fluid pressure difference between the injection and production wells decreases as the value of the highly permeable layer increases and in all cases the permeability of each layer affects the pore-fluid pressure drop between the injection and the production wells (Fig. 8).
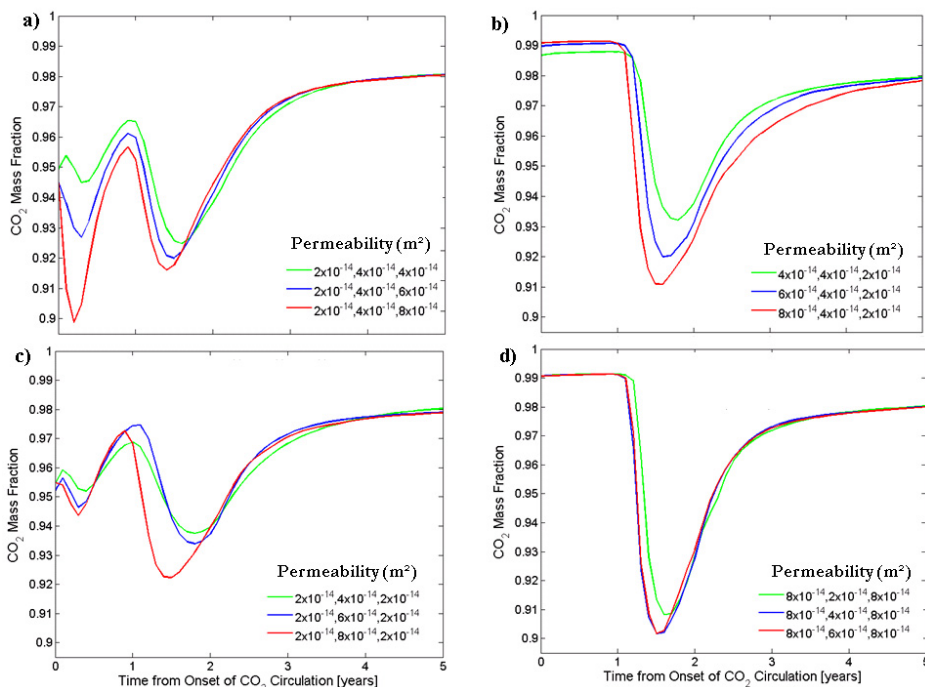
Fig. 7. Produced CO_2 mass fraction over time for different scenarios of a three-layered system: a) increasing permeability with layer depth, b) decreasing permeability with layer depth, c) high-permeability layer sandwiched between low-permeability layers, and d) low-permeability layer sandwiched between high-permeability layers.
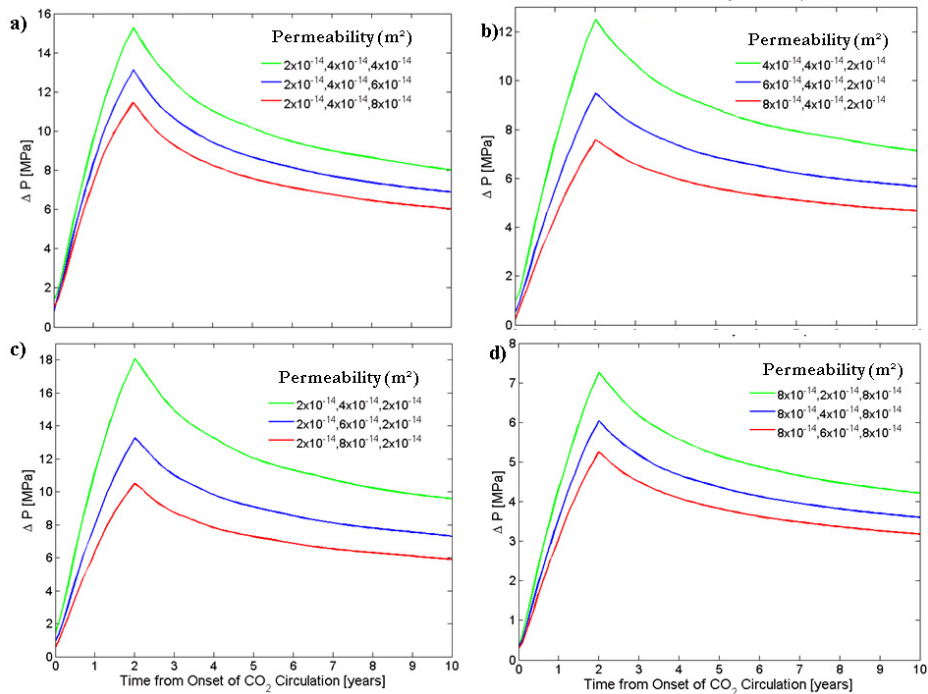
Fig. 8. Pore-fluid pressure drop between the injection and the production wells at the top of the reservoir, below the caprock versus time for different scenarios of a three-layered system: a) increasing layer-permeability with depth, b) decreasing layer-permeability with depth, c) high permeability layer sandwiched between low-permeability layers, and d) low-permeability layer sandwiched between high-permeability layers.

3.3. Four- Layered System

In the four-layered system simulated, we consider horizontal layers with varying permeability with a thickness of 12.5 m each. The different cases are: a) permeability increases with average layer depth, b) permeability decreases with average layer depth, c) alternating layers of low and high permeability, and d) alternating layers of high and low permeability.

The CO_2 mass fraction in the produced fluid and the pore-fluid pressure difference between the injection and production wells for different scenarios are shown in Figs. 9 and 10. Fig. 9a represents the CO_2 mass fraction in the produced fluid for the case where the low-permeability layer is at the top and the CO_2 mass fraction in the produced fluid varies as the bottom-layer permeability changes. When the high-permeability layer is at the top, the initial fluid composition is not affected by the permeability heterogeneity introduced by the layers, however, the minimum CO_2 mass fraction changes (Fig. 9b). When the high- and low-permeability layers are alternated, the CO_2 mass fraction decreases with increasing permeability of the second layer, regardless of the permeability of the top layer (Figs. 9c and 9d). Similar to the two- and three-layered systems, the pore-fluid pressure drop between the injection and the production wells decreases with an increase in permeability of any layer (Fig. 10).
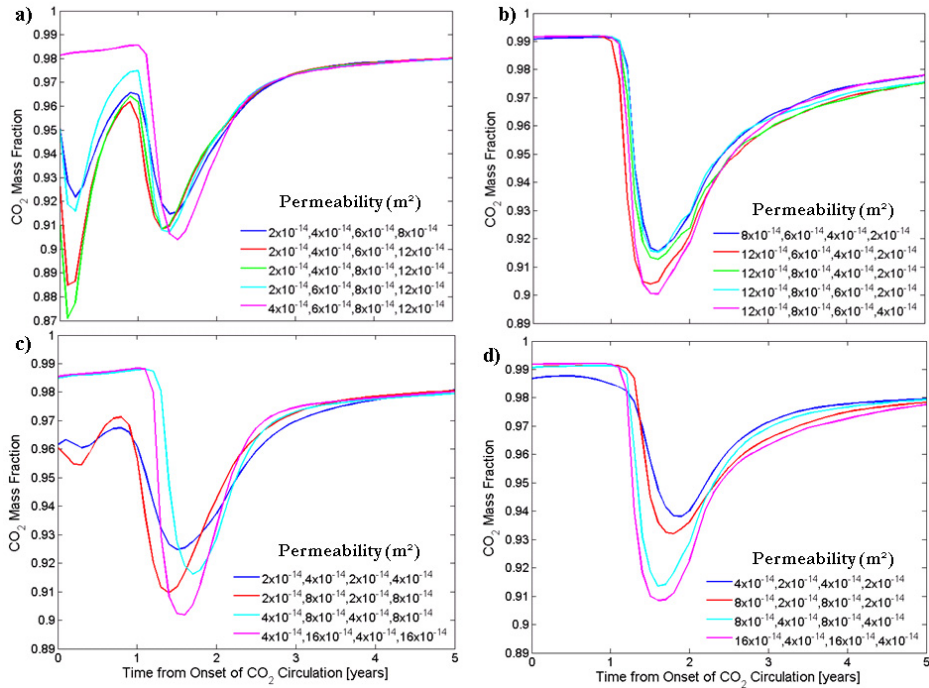
Fig. 9. Produced CO_2 mass fraction over time for different scenarios of a four-layered system: a) increasing layer permeability with depth, b) decreasing layer permeability with depth, c) alternating low- and high-permeability layers, and d) alternating high- and low-permeability layers.
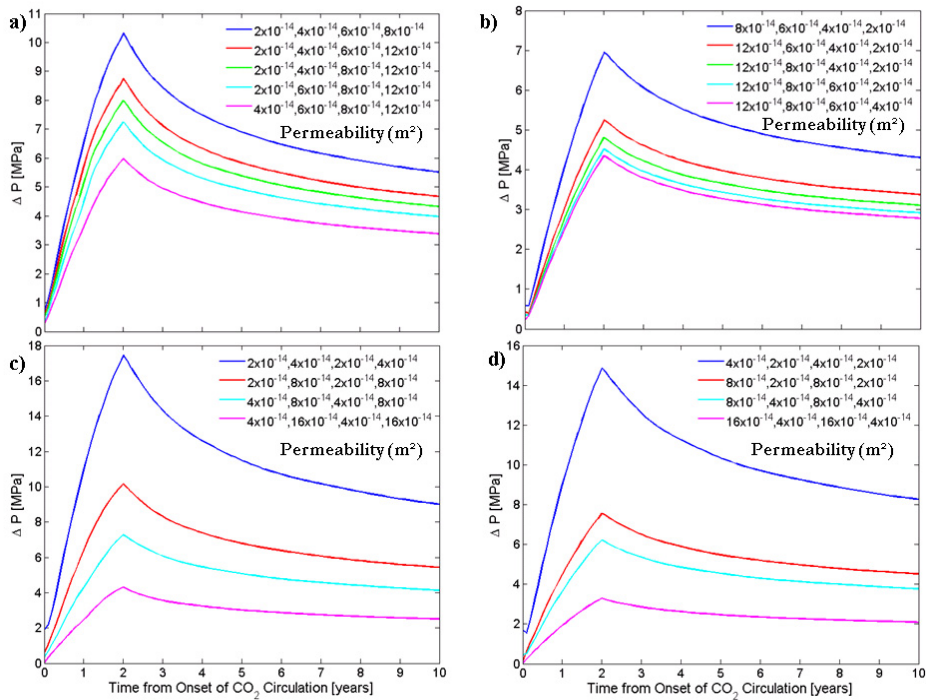

Fig. 10. Pore-fluid pressure drop between the injection and the production wells at the top of the reservoir below the caprock over time for different scenarios of a four-layered system: a) increasing layer-permeability with depth, b) decreasing layer-permeability with depth, c) alternating low- and high-permeability layers, and d) alternating high- and low-permeability layers.

4. Discussion

The CO_2 mass fraction in the produced fluid depends on the higher-permeability layers, whether they are located at the top or at the bottom of the reservoir (Figs. 11a and 11b). This result reflects the fact that the CO_2 moves predominantly in a horizontal direction from the injection to the production well so that horizontal layers constitute a system of conductors that are arranged in parallel with respect to the main CO_2 flow direction. The overall system permeability, or hydraulic conductivity, of such systems is dominated by the high-conductance layer and thus given by the arithmetic mean [16].
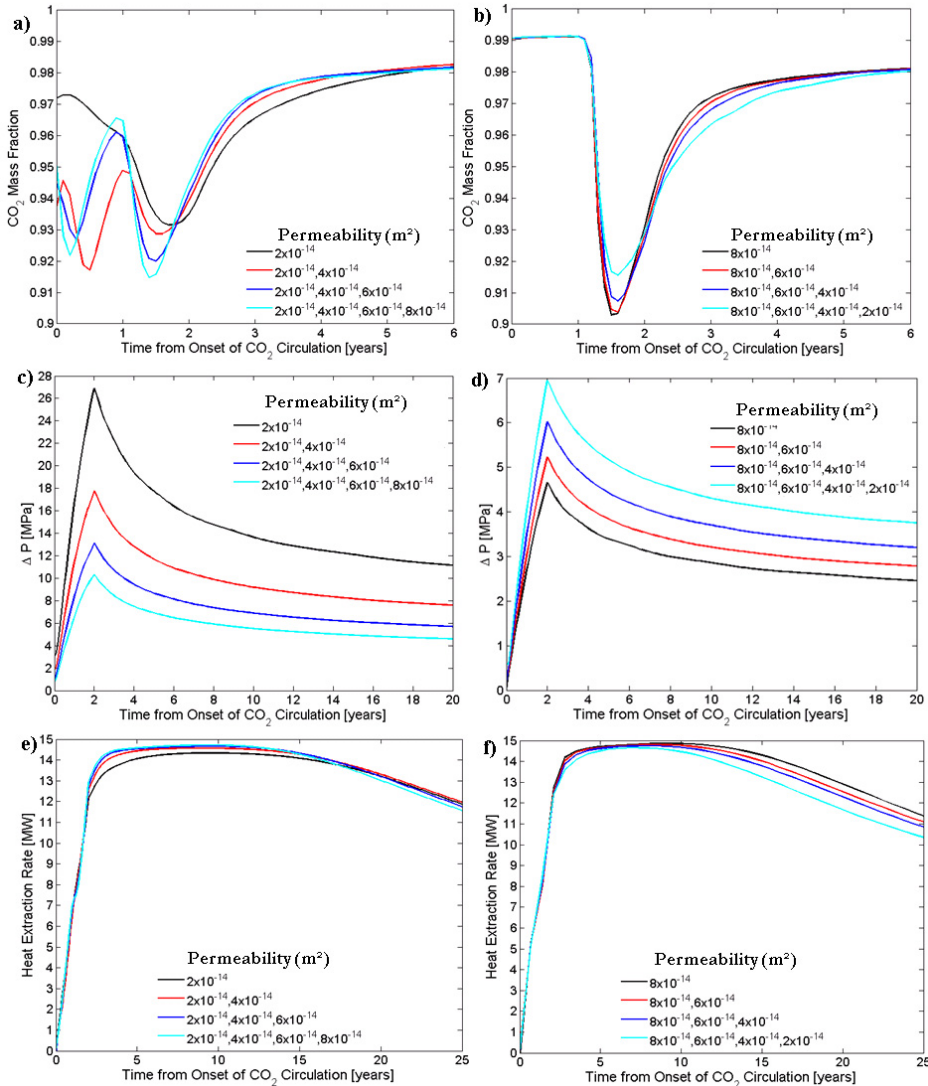
Fig. 11. Produced CO_2 mass fraction (a and b), pore-fluid pressure drop between injection and production wells at the top of the reservoir (c and d), and geothermal heat energy extraction (e and f) over time for increasing number of layers with the low-permeability layer at the top (left column) and the high-permeability layer at the top (right column).

The pore-fluid pressure drop between the injection and production wells is a function of permeability heterogeneity (Figs. 11c and 11d). The pressure drop is inversely proportional to the mobility (inverse kinematic viscosity) of the

CO_2. Therefore, systems with low pore-fluid pressure drops between the wells imply high mobility of CO_2. This results in a strong thermosiphon and reduces pumping power requirements [6]. The pore-fluid pressure drop between the wells in systems with low-permeability layers at the top of the reservoir is greater than in systems with high-permeability layers at the top.

The heat energy extraction rate from the geothermal reservoir (Figs. 11e and 11f) is independent of the permeability heterogeneity when the low-permeability layer is at the top of the reservoir. However, the heat energy extraction rate decreases as the number of high-permeability layers at the top increases.

5. Conclusions

This study shows the effect a multi-layered reservoir has on the CO_2 mass fraction in the produced fluid, the heat extraction rate over time, and the pore-fluid pressure evolution in the reservoir. We find that the produced CO_2 mass fraction is dominated by the high-permeability layers and their stratigraphic position within the reservoir. The heat extraction rate decreases as the permeability of the bottom layers decreases for different scenarios, but remains fairly constant as the permeability of the bottom layer increases. In all cases, the pore-fluid pressure drop between the injection and the production wells is affected by the permeability of the layers. This effect is more pronounced as the permeability of bottom layers increases for different scenarios. All of these effects change the pumping power requirements, if any [6], and the final power output of the geothermal system. Thus, permeability heterogeneity, in the form of layers, can have a considerable effect on the performance of a CO_2 Plume Geothermal (CPG) system.

Acknowledgements

Disclaimer

Drs. Randolph and Saar have significant financial and business interests in TerraCOH Inc, a company that may commercially benefit from the results of this research. The University of Minnesota has the right to receive royalty income under the terms of a license agreement with TerraCOH Inc. These relationships have been reviewed and managed by the University of Minnesota in accordance with its conflict of interest policies.

References

1.   Randolph, J.B. and M.O. Saar, *Coupling geothermal energy capture with carbon dioxide sequestration in naturally permeable, porous geologic formations: A comparison with enhanced geothermal systems*, in *Geothermal Research Council Transactions*. 2010. p. 433-438.
2.   Randolph, J.B. and M.O. Saar, *Coupling carbon dioxide sequestration with geothermal energy capture in naturally permeable, porous geologic formations: Implications for CO_2 sequestration.* Energy Procedia, 2011. **4**: p. 2206-2213.
3.   Randolph, J.B. and M.O. Saar, *Combining geothermal energy capture with geologic carbon dioxide sequestration.* Geophysical Research Letters, 2011. **38**(10).
4.   Saar, M.O., J.B. Randolph, and T.H. Kuehn, *Carbon dioxide-based geothermal energy generation systems*

and methods related thereto. 2012, U.S.Patents.

5. Buscheck, T.A., et al., *Integrated Geothermal-CO$_2$ Reservoir Systems: Reducing Carbon Intensity through Sustainable Energy Production and Secure CO$_2$ Storage.* Energy Procedia, 2013. **37**: p. 6587-6594.
6. Adams, B.M., et al., *On the importance of the thermosiphon effect in CPG (CO$_2$ plume geothermal) power systems.* Energy, 2014. **69**: p. 409-418.
7. Adams, B.M., et al., *A Comparison of Electric Power Output of CO$_2$ Plume Geothermal (CPG) and Brine Geothermal Systems for Varying Reservoir Conditions.* Applied Energy, 2014/15. **In Review**.
8. Dezayes, C., A. Genter, and G.R. Hooijkaas, *Deep-seated geology and fracture system of the EGS Soultz reservoir (France) based on recent 5km depth boreholes*, in *Proceedings of World Geothermal Congress*. 2005: Antalya, Turkey.
9. Atrens, A.D., H. Gurgenci, and V. Rudolph, *CO$_2$ Thermosiphon for Competitive Geothermal Power Generation.* Energy & fuels, 2009. **23**(1): p. 553-557.
10. Atrens, A.D., H. Gurgenci, and V. Rudolph, *Electricity generation using a carbon-dioxide thermosiphon.* Geothermics, 2010. **39**(2): p. 161-169.
11. Garapati, N., J.B. Randolph, and M.O. Saar, *Brine displacement by CO$_2$, energy extraction rates, and lifespan of a CO$_2$-limited, CO$_2$ Plume Geothermal system with a horizontal production well.* Geothermics, 2014/15. **In Review**.
12. Welch, P. and P. Boyle, *New Turbines to Enable Efficient Geothermal Power Plants.* Geothermal Resources Council Transactions, 2009.
13. Pruess, K., G. Moridis, and C. Oldenburg, *TOUGH2 user's guide, version 2.0*. 1999: Lawrence Berkeley National Laboratory Berkeley.
14. Pruess, K., *The TOUGH codes—A family of simulation tools for multiphase flow and transport processes in permeable media.* Vadose Zone Journal, 2004. **3**(3): p. 738-746.
15. Pruess, K., *ECO2N: A TOUGH2 fluid property module for mixtures of water, NaCl, and CO$_2$*. 2005: Lawrence Berkeley National Laboratory Berkeley.
16. Saar, M. and M. Manga, *Depth dependence of permeability in the Oregon Cascades inferred from hydrogeologic, thermal, seismic, and magmatic modeling constraints.* Journal of Geophysical Research: Solid Earth (1978–2012), 2004. **109**(B4).